#3

ANTIFERROMAGNETIC RESONANCE IN MANGANOUS CHLORIDE

DAVID H. DOUGLASS, JR.
M. W. P. STRANDBERG

TECHNICAL REPORT 362

SEPTEMBER 1, 1961

Reprinted from PHYSICA, Vol. 27, pp. 1-17, 1961.

MASSACHUSETTS INSTITUTE OF TECHNOLOGY
RESEARCH LABORATORY OF ELECTRONICS
CAMBRIDGE, MASSACHUSETTS

The Research Laboratory of Electronics is an interdepartmental laboratory of the Department of Electrical Engineering and the Department of Physics.

The research reported in this document was made possible in part by support extended the Massachusetts Institute of Technology, Research Laboratory of Electronics, jointly by the U. S. Army (Signal Corps), the U. S. Navy (Office of Naval Research), and the U. S. Air Force (Office of Scientific Research, Air Research and Development Command), under Signal Corps Contract DA36-039-sc-78108, Department of the Army Task 3-99-20-001 and Project 3-99-00-000, and was performed under Signal Corps Contract DA36-039-sc-87376.

Douglass, Jr., David H.
Strandberg, M. W. P.
1961

Physica 27
1–17

ANTIFERROMAGNETIC RESONANCE IN MANGANOUS CHLORIDE *

by DAVID H. DOUGLASS JR. **) and M. W. P. STRANDBERG

Department of Physics and Research Laboratory of Electronics Massachusetts Institute of Technology Cambridge, Massachusetts, U.S.A.

Synopsis

The molecular fields and linewidths of antiferromagnetic manganous chloride were measured by magnetic resonance techniques as a function of temperature, frequency, and orientation. Demagnetization effects were observed. The "10/3 effect" was observed for the paramagnetic state. An effect similar to this was observed in the antiferromagnetic state.

1. *Introduction.* The technique of magnetic resonance has developed into a powerful means for unraveling the properties of matter. It has been used, with considerable success, to study and measure some of the properties of antiferromagnetic materials. In this investigation, it was used to study crystalline manganous chloride in both the paramagnetic and antiferromagnetic states. Murray and Roberts [1)2)] have shown by specific heat and susceptibility measurements that manganous chloride undergoes phase transitions at 1.96°K and 1.81°K; and Wollan [3)], using neutron scattering found that the transition at 1.96°K was from the paramagnetic state to the antiferromagnetic state (State I) and the transition at 1.81°K was to a second antiferromagnetic modification (State II). He also showed that this second transition was strongly field-dependent. This effect is illustrated in fig. 1. He was able to explain all of his results by using the two-sublattice model and the concept of antiferromagnetic domains. The domain structure of State I with and without a magnetic field is shown in figs. 2 and 3. A field of approximately 200–1000 gauss was sufficient to convert the crystal into a single domain. The magnetic fields and frequencies used in these experiments were such that only State I in the single domain modification was observed. (See fig. 1).

---

*) This work was supported in part by the U.S. Army (Signal Corps.), the U.S. Air Force (Office of Scientific Research, Air Research and Development Command), and the U.S. Navy (Office of Naval Research).

**) Present address: Massachusetts Institute of Technology, Lincoln Laboratory. Lexington, Massachusetts.

The crystal structure is a hexagonal layer structure [4]) of the $CdCl_2$ class. The manganous ions are arranged in a hexagonal pattern in a sheet. This

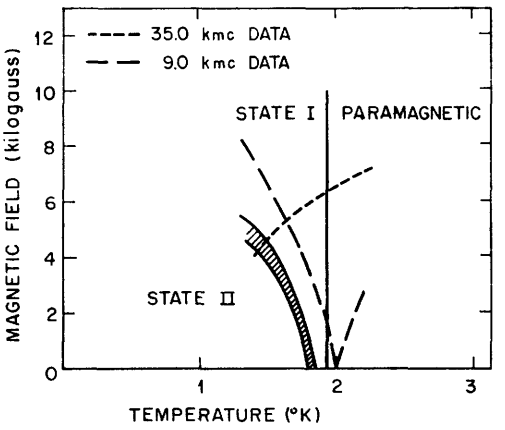

Fig. 1. Magnetic "phase" diagram for manganous chloride. Field perpendicular to a-axis.

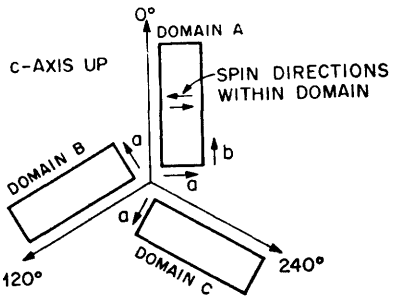

Fig. 2. Domains in manganous chloride; no magnetic field. State I ($1.81 < T < 1.96$°K)

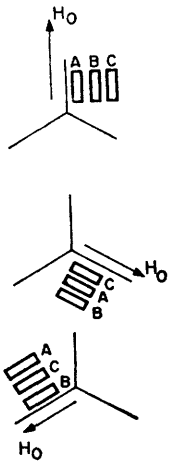

Fig. 3. Domains in manganous chloride in the presence of a magnetic field. State I.

sheet is sandwiched between two similar sheets of chlorine ions, and the c-axis is normal to these sheets. The unit cell is rhombohedral ($a = 6.20$ A°, $\alpha = 34°35'$) with a manganous ion at (0, 0, 0) and chlorine ions at (u, u, u)

and $(\bar{u}, \bar{u}, \bar{u})$ with $u \approx 0.25$. The single crystals, which are transparent and pink, are very easily cleaved parallel to the above-mentioned sheets. Samples can be prepared in the form of thin disks, with the c-axis normal to the plane of the disk.

2. *Theory.* Resonance Equations. Since Wollan was able to explain his data by using the two-sublattice model, the same model is assumed here. Kittel [5]) and Nagamiya [6]) have shown that the equations of motion are

$$\dot{\boldsymbol{M}}_1 = \gamma \boldsymbol{M}_1 \times \boldsymbol{H}_{\text{eff}_1} \tag{1a}$$

$$\dot{\boldsymbol{M}}_2 = \gamma \boldsymbol{M}_2 \times \boldsymbol{H}_{\text{eff}_2} \tag{1b}$$

where $\boldsymbol{H}_{\text{eff}_1}$ and $\boldsymbol{H}_{\text{eff}_2}$ are defined as

$$\boldsymbol{H}_{\text{eff}_1} = \boldsymbol{H}_0 + \boldsymbol{H}_{A_1} + \boldsymbol{H}_{\text{rf}} - \lambda \boldsymbol{M}_2 - N_x(M_1{}^x + M_2{}^x)\,\boldsymbol{j}_x - N_y(M_1{}^y + M_2{}^y)\,\boldsymbol{j}_y - N_z(M_1{}^z + M_2{}^z)\boldsymbol{j}_z \tag{2a}$$

$$\boldsymbol{H}_{\text{eff}_2} = \boldsymbol{H}_0 + \boldsymbol{H}_{A_2} + \boldsymbol{H}_{\text{rf}} - \lambda \boldsymbol{M}_1 - N_x(M_1{}^x + M_2{}^x)\,\boldsymbol{j}_x - N_y(M_1{}^y + M_2{}^y)\,\boldsymbol{j}_y - N_z(M_1{}^z + M_2{}^z)\,\boldsymbol{j}_z. \tag{2b}$$

The quantity $\boldsymbol{H}_0$ is the external field; $\boldsymbol{H}_{A_1}$ and $\boldsymbol{H}_{A_2}$ are the anisotropy fields for sublattices 1 and 2, respectively: $\boldsymbol{H}_{\text{rf}}$ is the rf field; $\lambda \boldsymbol{M}$ represents the exchange interaction between the two sublattices; and the last three terms are the corrections that result from demagnetization effects. Until now, demagnetization effects have never been important experimentally in antiferromagnetism. This investigation shows that for these experiments the effects are large and cannot be neglected.

Because solutions of equations 1 depend on the shape of the sample, there are three cases of experimental interest for a disk-shaped sample; they are shown in fig. 4. The solutions of the equations are given in appendix A, and only the results are presented here.

Case I

$$H_0 \approx \frac{[(\omega/\gamma)^2 - 2H_E H_A]^{\frac{1}{2}}}{1 - 4\pi\chi} \tag{3}$$

Case II

$$H_0 \approx \left[\frac{(\omega/\gamma)^2 - 2H_E H_A}{1 + 4\pi\chi}\right]^{\frac{1}{2}} \tag{4}$$

Case III

$$H_0 \approx |(\omega/\gamma) \pm (2H_E H_A)^{\frac{1}{2}}|, \quad T < T_N \tag{5}$$

where ω is the angular frequency of the rf field, χ is the appropriate susceptibility, and H_E is equal to $\lambda|\boldsymbol{M}_{1,2}|$. Note that equations 3 and 4 are also descriptions of the paramagnetic state when $2H_E H_A$ is equal to zero.

Paramagnetic linewidth. Van Vleck [7]) has considered a special

case of paramagnetic linewidths in crystals by the method of moments. In general this method breaks the Hamiltonian into three parts, $\mathscr{H}_0 + \mathscr{H}' + \mathscr{H}''$; where $\mathscr{H}_0$ is the sum of the single-spin (Zeeman, crystalline field, and so forth) operators, the two spin (dipole-dipole, exchange) operators which commute with the single-spin operators, and the transition-inducing operator S_x. $\mathscr{H}'$ and $\mathscr{H}''$ are, in the eigen-representation of $\mathscr{H}_0$, the parts of the Hamiltonian which do and do not commute with the single spin operators and which do not commute with S_x. The effect of $\mathscr{H}'$ is to broaden the sharp lines that would occur if there were no interactions; $\mathscr{H}''$ produces weak satellite lines by mixing the single-spin eigen-states. These satellite lines contribute to the mean square absorption frequency, but not to the individual linewidths when these satellites are resolved and hence are usually of no experimental interest. To eliminate their contribution in the theoretical calculation of the moments of resonant absorption lineshape a truncated Hamiltonian $\overline{\mathscr{H}} = \mathscr{H}_0 + \mathscr{H}'$ and a suitably truncated spin operator $\bar{S}_x$ must be used. It is obvious that the form of $\mathscr{H}_0$ will determine how the interaction Hamiltonian will separate into its two parts, and hence will determine the value of the linewidth.

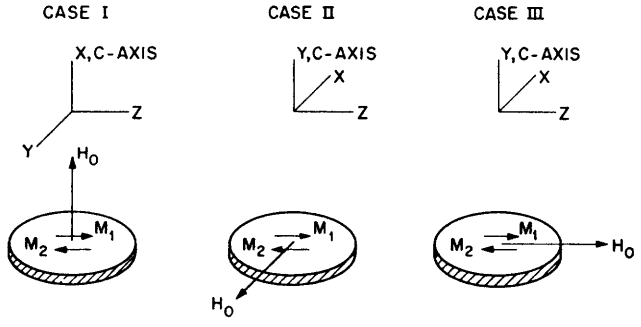

Fig. 4. The three spacial orientations of interest in manganous chloride.

Van Vleck considered the case of a Zeeman spin system in an external field under the influence of exchange and dipolar interactions. His calculations give a linewidth that is independent of exchange. It is not clear, however, that this Hamiltonian will describe the $MnCl_2$ system because an electrostatic interaction probably exists. Ishiguro [8]) has added an electrostatic interaction (zero-field splitting) under the conditions that it is larger than the dipolar and exchange interactions. In this case, the truncation is carried out differently, and the linewidth is found to depend upon the exchange term. This case does not apply to $MnCl_2$ either, because here the electrostatic interaction is smaller than the dipolar and the exchange interactions. Murray and Roberts estimate the electric interaction at 0.06 cm^{-1} while the dipolar and exchange energies are 0.2 cm^{-1} and 0.6 cm^{-1}.

Because the electrostatic interaction is small, the Van Vleck-truncated

Hamiltonian is used here as the best approximation for the case where the Zeeman energy is greater than the exchange energy. This case can be suitable modified when this condition does not hold.

Since the exchange energy is large compared to both the dipolar and electric field energies, exchange narrowing effects must be considered.

Anderson and Weiss [9]) have considered the Van Vleck case (simple dipolar interaction) under the condition that the operating frequency could be larger than the exchange frequency. They showed that if $\nu_0 \gg \nu_e$, then the halfwidth is

$$\Delta\nu = \frac{h}{|J|}\langle\Delta\nu_d^2\rangle = \frac{\langle\Delta\nu_d^2\rangle}{\nu_e} \tag{6}$$

where $\Delta\nu_d$ is the halfwidth obtained by Van Vleck, J is the exchange integral, ν_0 is the rf frequency, and $|J|/h = \nu_e$. However, if $\nu_0 \ll \nu_e$, then

$$\Delta\nu = \tfrac{10}{3}\frac{h}{|J|}\langle\Delta\nu_d^2\rangle = \tfrac{10}{3}\frac{\langle\Delta\nu_d^2\rangle}{\nu_e}. \tag{7}$$

Equations 6 and 7 predict a variation in dipolar halfwidth with rf frequency by a factor of 10/3; Anderson and Weiss call this the "10/3 effect".

Kubo and Tomita [10]) and Yokota [11]) have considered the same problem. They started from a more fundamental point of view, worked the problem out in more detail, and obtained the full frequency dependence. For the simple case of spin $\frac{1}{2}$ and "good symmetry", they get for the halfwidth

$$\Delta\nu = \frac{\langle\Delta\nu_d^2\rangle}{\nu_e}\left[1 + \tfrac{2}{3}\,e^{-\frac{1}{2}(\nu_0/\nu_e)^2} + \tfrac{5}{3}\,e^{-2(\nu_0/\nu_e)^2}\right] \tag{8}$$

It can be seen that equation 8 reduces to equations 7 and 6 in the corresponding limits. A variation of linewidth with frequency has been observed in aqueous copper potassium chloride [12]) ($CuK_2Cl_4.2H_2O$) and in diphenyl picryl hydrazyl [13]). In both cases, this is attributed to the 10/3 effect. Since for $MnCl_2$ the zero field splitting is probably small compared to the dipolar energy, we feel thar these calculations are relevant to our case, and we will use eq. 8 to discuss the frequency dependence of the paramagnetic linewidth.

As for the explicit temperature dependence of the paramagnetic linewidth, we note that Pryce and Stevens [14]) have considered the temperature dependence of the halfwidth and they have shown that the explicit temperature dependence arises from an exponential operator arising from the Boltzmann distribution of the diagonal elements of that density matrix.

The first temperature dependent term in the expansion of the exponential weighting factor for the second moment is of the form

$$\Sigma\frac{\langle 1\,|W_{ij}|\,2\rangle\,\langle 2\,|W_{ij}|\,3\rangle\,\langle 3\,|W_{ij}|\,1\rangle}{kT} \tag{9}$$

where W is the appropriate term in the Hamiltonian. Therefore, the temperature dependence of the linewidth should have the asymptotic form

$$\langle \Delta\nu^2 \rangle^{\frac{1}{2}} \propto 1 + \frac{A}{T} \simeq e^{A/T} \tag{10}$$

where A is a constant that depends on the matrix elements in eq. 9.

The value of A depends on the nature of the Hamiltonian and how it is truncated. It would thus appear that the truncation is independent of temperature in the paramagnetic state, and for that reason the "10/3 effect" can be factored from the temperature effects. Note well that the 10/3 factor depends upon the form of $\mathscr{H}'$ and $\mathscr{H}''$, that is, on the dipolar energy and crystalline zero field splitting. This factor should change, therefore, depending on the relative magnitudes of the crystalline and dipolar terms. Since our results also indicate that the crystalline zero field splitting is smaller than the dipolar term, Eq. 8 will be used to describe the effect of frequency on the linewidth. Because exchange is the largest term in the Hamiltonian, one would expect that $A \sim J/k \sim T_N$.

More precisely, we find that the leading term in the temperature dependence of the *rms* linewidth should be $T_N/2T$ or $\frac{1}{2}$ in units of T_N/T. This calculation can have little relevance to the present case, however, since the observed *rms* linewidth has a variable slope versus T_N/T. At large T_N/T, where the leading term should be adequate, the variation is greater than $\frac{1}{2}$. At smaller T_N/T, the slope approaches T_N/T, although here the leading term should become inadequate. Quite possibly, the trouble here is due to the *implicit* temperature dependence of the terms which give rise to the *explicitly* temperature dependent terms, such as the crystalline splitting. Ignorance of implicit temperature dependence (or whatever the cause of the inadequacy of the theory is) has prompted us to forego further theoretical development here (however, we are continuing these investigations), and to gratefully accept and indicate the qualitative agreement only.

With the above reservations in mind, the complete expression we will use for the paramagnetic linewidth in $MnCl_2$ is

$$\Delta\nu = \frac{\langle \Delta\nu_d \rangle^2}{\nu_e} [1 + \tfrac{2}{3} e^{-\frac{1}{2}(\nu_0/\nu_e)^2} + \tfrac{5}{3} e^{-2(\nu_0/\nu_e)^2}] [e^{A/T}] \tag{11}$$

Antiferromagnetic linewidth. Nethercot and Johnson [15] present a result that was obtained by Townes for the halfwidth in an antiferromagnetic material. It is derived by relating fluctuations in the molecular fields to the spread in resonant fields. The result is

$$\Delta\nu = \frac{2\nu_A(0)}{n} [B_S^{-1}(T/T_N) - B_S(T/T_N)] \tag{12}$$

where $\nu_A(0)$ is the frequency corresponding to the value of the anisotropy field at $T = 0$, $B_S(T/T_N)$ is the modified Brillouin function of spin S (in

this case $S = \frac{5}{2}$), and n is the equivalent number of nearest neighbors of spin $\frac{1}{2}$ (i.e., 6 neighbors of spin $\frac{5}{2}$ are equivalent to 30 neighbors of spin $\frac{1}{2}$).

Nethercot and Johnson found that for MnF_2, equation 12 gave results that were too small by a factor of 5. In the derivation of equation 12, exchange narrowing was assumed. (This assumption should be checked theoretically). If exchange narrowing can be assumed, then the "$\frac{10}{3}$ effect" should be included for consistency, and as a result, the complete expression for the halfwidth would be

$$\Delta\nu = \frac{2\nu_A(0)}{n}\left[B_S^{-1}(T/T_N) - B_S(T/T_N)\right]\left[1 + \tfrac{2}{3}\, e^{-\frac{1}{2}(\nu_0/\nu_e)^2} + \tfrac{5}{3}\, e^{-2(\nu_0/\nu_e)^2}\right] \qquad (13)$$

For the frequencies used in the MnF_2 experiments, this expression would give a factor of 10/3 greater than that given by equation 12. Nethercot and Johnson have interpreted equation 12 as the full linewidth; this puts them in error by a factor of 2. This factor of 2 when combined with the factor of 10/3 just about accounts for the above-mentioned factor of 5. Similarly, they apply equation 12 to the results on aqueous copper chloride [16], ($CuCl_2.2H_2O$), and find the calculation too small by approximately a factor of 8. Here again the frequencies are such that the 10/3 effect would apply; this effect when combined with the factor of 2 fairly well accounts for the factor 8. In this case, the question of whether or not the frequency dependence can be separated from the temperature dependence is pertinent.

3. *Results. a.* Resonant Field vs. Temperature and Frequency. Measurements were made at 9.0 kmc and 35.0 kmc as a function of temperature and orientation. The values of the resonant field for the two frequencies are shown in figs. 5 and 6. The experimental setup is described in appendix B.

For temperatures greater than approximately 7°K, the system is entirely paramagnetic, and the molecular field quantity $2H_E H_A$ is zero. By substituting the appropriate values of $\chi(T)$ into equations 3 and 4, it is found that there is perfect agreement between the experimental and the calculated values.

However, at lower temperatures, the molecular field quantity $2H_E H_A$ is not zero and, therefore, must be considered. It is necessary to know the susceptibility as a function of field as well as temperature in order to measure this quantity. Unfortunately, Murray and Roberts measure it only to values of 2600 gauss, whereas some of our data points were as high as 15,000 gauss. However, it was possible to use data that did not exceed 4000 gauss by selecting certain portions of the experimental curves. The low field values of the susceptibility were then used to calculate the quantity $2H_E H_A$ as a function of temperature. Thus curve is shown in fig. 7. As a check, the values of $2H_E H_A$ thus obtained were substituted back into the equations along with the low field susceptibilities, and the resonant field

was calculated. These calculated values are shown in figs. 5 and 6 by a solid line. Agreement is rather poor at high values of H/T. This is not surprising, for in the derivation of the resonance equations, we assume that $M=\chi(T)H$. This certainly cannot be true for arbitrarily large H or small T.

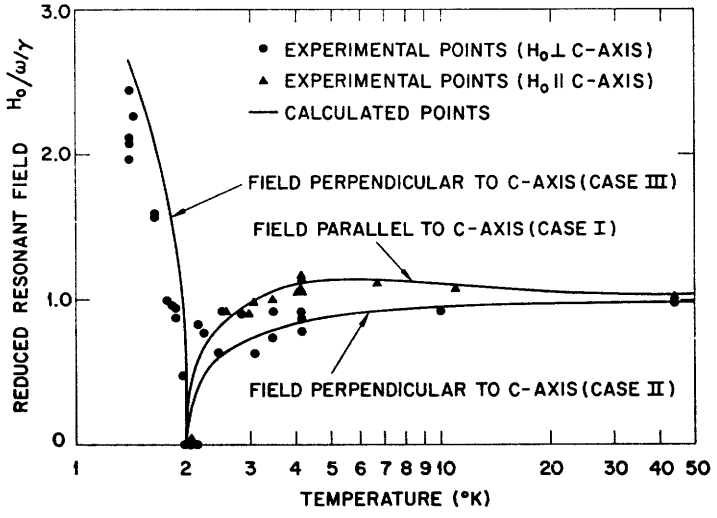

Fig. 5. Reduced resonant field vs. temperature at 9.0 kmc.

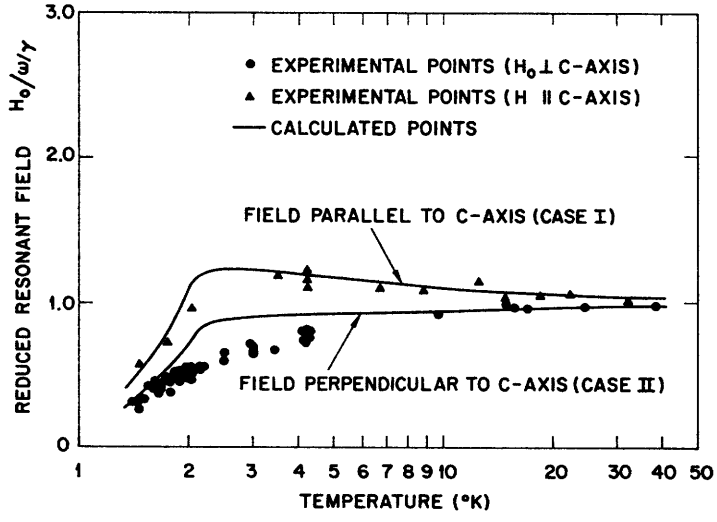

Fig. 6. Reduced resonant field vs. temperature at 35.0 kmc.

Because of the nature of the domain orientation with respect to magnetic field (see fig. 3), orientation of the sample, in such a way that the spin direction would be parallel to the magnetic field, would seem to be impossible. (Case III in fig. 4.) However, the solutions for the resonant field for the two possible orientations where H_0 is perpendicular to the spins can become imaginary. This situation occurs at 9.0 kmc and at the lowest temperatures;

however, a weak resonance *was* observed (Fig. 5). The interpretation is that most of the domains are perpendicular to the external field, but that a few are parallel. When the resonance due to the perpendicular domains becomes imaginary, the resonance from the parallel ones dominates. Since this occurs only at the lowest temperatures, it was necessary to solve the equations for this orientation only in the limit $T < T_N$.

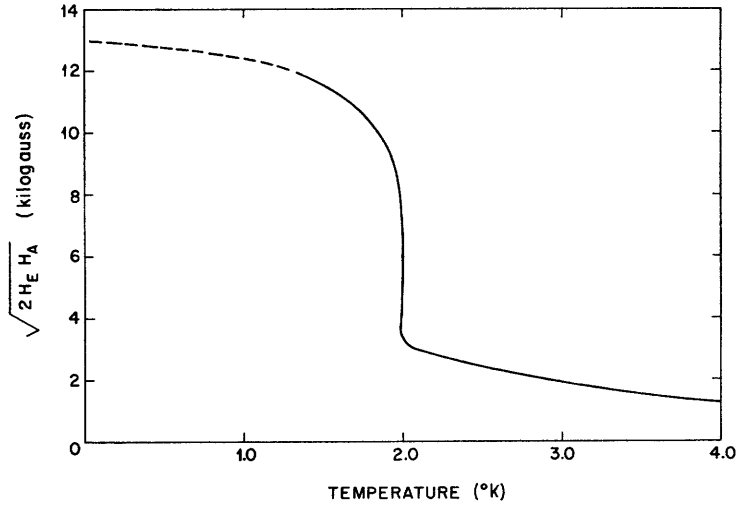

Fig. 7. $(2H_EH_A)^{\frac{1}{2}}$ vs. temperature.

Examination of the plot of $(2H_EH_A)^{\frac{1}{2}}$ versus temperature in fig. 7 shows that the molecular fields have large values well above the transition temperatures. Perhaps this can be explained by or connected to the fact that there is considerable short-range order in the system above the Néel temperature. Just above the Néel temperature, the spin entropy has attained only 70 per cent of its maximum value, and at 4.2°K it has attained only 90 per cent. An extrapolation to $T = 0$ gives $(2H_EH_A)^{\frac{1}{2}}$ equal to approximately 13 kilogauss. A value for H_A of 5 kilogauss is obtained by using $H_E = 17$ kilogauss.

For Case II in fig. 4, the resonance was observed as a function of rotation about the C-axis. There was a slight variation with angle that showed a 60° periodicity, which is the variation that would be expected on the basis of the domain structure given in figs 2 and 3.

Because the samples could be prepared in the form of thin platelets, the spin wave resonances were looked for, but without success. Theoretical calculations [17]) show, however, than the separation of the spin wave resonances was much less than the linewidth under the experimental conditions used.

b. Linewidths. Experimentally, the halfwidth was taken to be the difference between the field at the higher inflection point and the field at

the maximum of the absorption versus field curve. Also, because the field, rather than frequency, was swept, the usual correction factor $\partial\nu/\partial H$ was applied to the experimental values.

The corrected values of the halfwidth are shown in figs. 8 and 9. There was no consistent orientation dependence. The field quantities $\Delta\nu_d$ and ν_e have been determined [9]) to be 4.9 kmc and 45 kmc, respectively. These values would make the frequency factor in eq. 11 equal to 10/3 for $\nu_0 = 9.0$ kmc and equal to 2.0 for $\nu_0 = 35.0$ kmc.

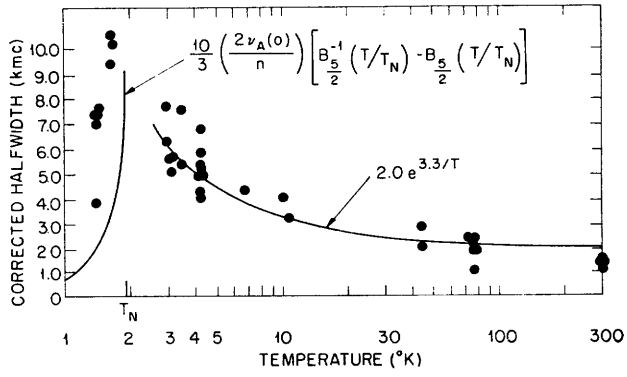

Fig. 8. Halfwidth vs. temperature at 9.0 kmc.

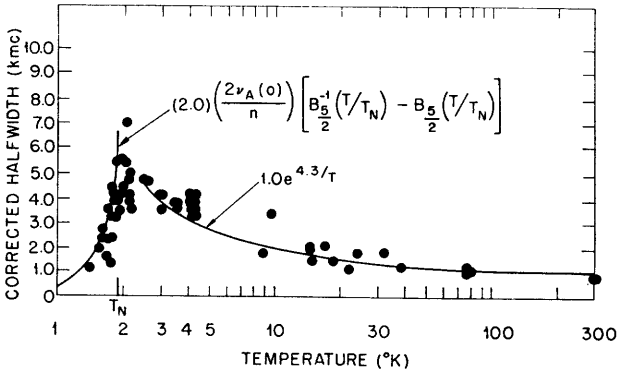

Fig. 9. Halfwidth vs. temperature at 35.0 kmc.

Examine first the linewidths in the paramagnetic region. It is seen that the temperature dependence can apparently be fitted with a curve of the form of eq. 10, and that the line is narrower at the higher frequency in agreement with the 10/3 effect. A quantitative comparison shows that the ratio of the experimental linewidths is approximately 2 and is almost independent of temperature, whereas the ratio predicted by eq. 11 is approximately 1.6. Note that A is approximately equal to T_N, as expected. Experimentally, the values for the coefficient of the temperature varying factor (see figs. 8 and 9) are 2.0 kmc and 1.0 kmc for ν_0 equal to 9.0 kmc and 35.0 kmc, respectively. These values should be compared with the values 1.7 kmc and 1.0 kmc given by eq. 11.

In the antiferromagnetic region, eq. 13 fits the data very well for 35.0 kmc by using $\nu_A(0) = 14$ kmc and n equal to $5 \times 6 = 30$. The agreement for $\nu_0 = 9.0$ kmc is not as good. At this frequency, however, the experimental linewidths near $T = 2°K$ are very large, and $\partial\nu/\partial H$ is nearly to zero, with the result that their product is uncertain. (The linewidths in the region

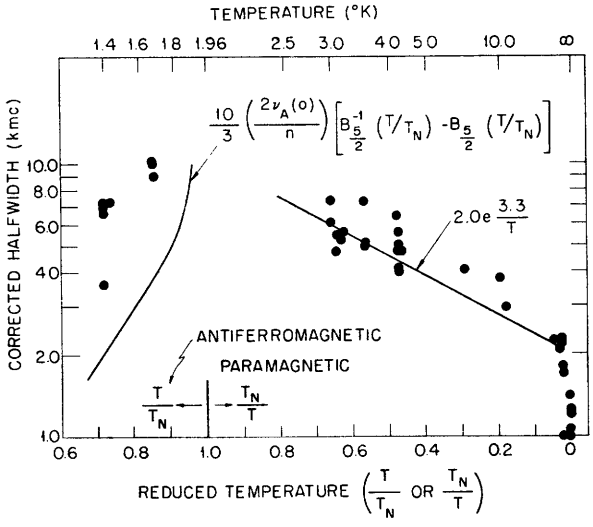

Fig. 10. Halfwidth vs. temperature at 9.0 kmc.

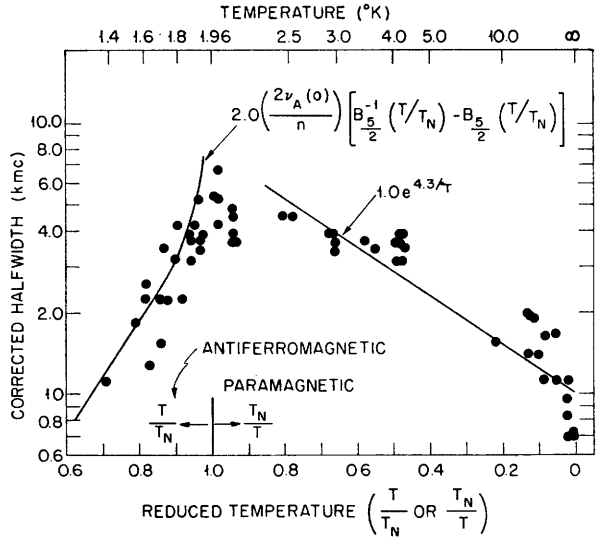

Fig. 11. Halfwidth vs. temperature at 35.0 kmc.

1.7–2.5°K could not be determined). It is certain, however, that there is a definite variation in halfwidths with frequency.

We would like to propose the following method of displaying linewidth data as a function of temperature as being more useful than the conventional method. In figs. 10 and 11, the logarithm of the linewidth is plotted versus

T/T_N or T_N/T, depending on whether T is above or below T_N. (Figs. 10 and 11). This representation has the following advantages: an exponential variation of the linewidth as T approaches T_N is displayed as a straight line; the region near the transition temperature is expanded; and temperatures from zero to infinity can be plotted on a finite sheet of paper.

From figs. 8 and 9, we can see that on a conventional plot, an exponential variation of linewidth with temperature above T_N appears to fit quite well. However, when the same data are plotted in the proposed way (Figs. 10 and 11), it is seen that an exponential does *not* fit the data very well. Perhaps one reason is that over this temperature range, the implicit temperature dependence of various parameters (exchange integral, electrostatic interaction, and so on) may be important. It is also noticed that the Townes' expression for the antiferromagnetic halfwidth can be approximated by an exponential over a good part of its range.

4. *Summary of experimental results.* This work reports on the magnetic resonance investigation of antiferromagnetic manganous chloride at 9.0 kmc and 35.0 kmc as a function of temperature and orientation. Demagnetization effects were found to be important. A value of 13.000 gauss was found for $(2H_EH_A)^{\frac{1}{2}}$ at $T = 0$, and therefore $H_A(0)$ has a value of 5000 gauss.

The effect of line narrowing when the rf frequency was increased was observed at all temperatures in both the antiferromagnetic state and the paramagnetic state. In the paramagnetic state at high temperatures this is called the 10/3 effect. The temperature dependence of the paramagnetic linewidth was found to vary qualitatively as $e^{A/T}$. In the antiferromagnetic state, the expression by Townes seems adequate.

APPENDIX A.

Solutions of the equation of motion. Because equations 1*a* and 1*b* are nonlinear, the method of small oscillations is applied to linearize them. This is done by letting $\boldsymbol{M}_1 \rightarrow \boldsymbol{M}_{10} + \delta\boldsymbol{M}_1$ and $\boldsymbol{M}_2 \rightarrow \boldsymbol{M}_{20} + \delta\boldsymbol{M}_2$, where $\boldsymbol{M}_{10}$ and $\boldsymbol{M}_{20}$ are the values of $\boldsymbol{M}_1$ and $\boldsymbol{M}_2$ in the absence of $\boldsymbol{H}_{\mathrm{rf}}$. The quantities $\delta\boldsymbol{M}_1$ and $\delta\boldsymbol{M}_2$ are assumed to have time dependence $e^{i\omega t}$, where ω is the angular frequency of the rf field. The term containing $\boldsymbol{H}_{\mathrm{rf}}$ is now dropped as being small in magnitude compared with the other terms. The equations, when expanded, will become linear.

Case I: $\quad H_A \| Z,\ H_0 \| X,\ N_x = 4\pi,\ N_y = N_z = 0.$

For this case, equations 1*a* and 1*b* can be represented by a single matrix equation:

$$\begin{bmatrix}
\frac{-i\omega}{\gamma} & 0 & H_A-\lambda M_{20^z} & \lambda M_{10^z} & \lambda M_{20^y} & -\lambda M_{10^y} \\
0 & \frac{-i\omega}{\gamma} & \lambda M_{20^z} & -H_A-\lambda M_{10^z} & -\lambda M_{20^y} & \lambda M_{10^y} \\
-H_A+\lambda M_{20^z} & -(\lambda+N)M_{10^z} & \frac{-i\omega}{\gamma} & 0 & H_0-\lambda M_{20^x} & \lambda M_{10^x} \\
-NM_{10^z} & & & & -N(M_{10^x}+M_{20^x}) & \\
-(\lambda+N)M_{20^z} & H_A+\lambda M_{10^z} & 0 & \frac{-i\omega}{\gamma} & \lambda M_{20^x} & H_0-\lambda M_{10^x} \\
 & -NM_{20^z} & & & & -N(M_{10^x}+M_{20^x}) \\
-\lambda M_{20^y}+NM_{10^y} & (\lambda+N)M_{10^y} & -H_0+\lambda M_{20^x} & -\lambda M_{10^x} & \frac{-i\omega}{\gamma} & 0 \\
 & & +N(M_{10^x}+M_{20^x}) & & & \\
(\lambda+N)M_{20^y} & NM_{20^y}-\lambda M_{10^y} & -\lambda M_{20^x} & -H_0+\lambda M_{10^x} & 0 & \frac{-i\omega}{\gamma} \\
 & & & +N(M_{10^x}+M_{20^x}) & &
\end{bmatrix}
\begin{bmatrix} \delta M_{1^x} \\ \delta M_{2^x} \\ \delta M_{1^y} \\ \delta M_{2^y} \\ \delta M_{1^z} \\ \delta M_{2^z} \end{bmatrix} = 0 \qquad \text{A-1)}$$

As is well known, the only way for the eigenvector

$$\begin{bmatrix} \delta M_1 \\ \delta M_2 \end{bmatrix}$$

to have nonzero values is for the determinant of the matrix to be equal to zero. This, in general, will lead to a polynomial in ω of degree 6. The six roots of this polynomial will be the eigenfrequencies of the system. For this case,

$$M_{10^y} = M_{20^y} = 0, \; M_{10^x} = M_{20^x}, \; M_{10^z} = -M_{20^z}.$$

Also, the following definitions are used:

$$\lambda M_{10^z} = -H_E \text{ and } M_{10^x} = \frac{\chi H_0}{2}.$$

By expanding the determinant and collecting terms, we find that

$$(\omega/\gamma)^2 = (1 - 4\pi\chi)^2 H_0^2 + 2H_E H_A + H_A^2 \qquad \text{(A-2)}$$

$$(\omega/\gamma)^2 = (1 - (\lambda + 4\pi)\chi)^2 H_0^2 + 2H_E H_A + H_A^2 + (8\pi/\lambda) H_E H_A \qquad \text{(A-3)}$$

$$(\omega/\gamma)^2 = 0. \qquad \text{(A-4)}$$

Solving these equations for H_0 gives

$$H_0 = \pm \frac{[(\omega/\gamma)^2 - 2H_E H_A - H_A^2]^{\frac{1}{2}}}{1 - 4\pi\chi} \qquad \text{(A-5)}$$

$$H_0 = \pm \frac{[(\omega/\gamma)^2 - 2H_E H_A - H_A^2 - (8\pi/\lambda) H_E H_A]^{\frac{1}{2}}}{1 - (\lambda + 4\pi)\chi} \qquad \text{(A-6)}$$

Kittel[18] has shown that $\lambda \approx (1/\chi_\perp)$, where $\chi_\perp$ is the susceptibility perpendicular to H_A; so solution of equation A-6 occurs at high fields and can be dropped. Thus the only solution of interest is the positive root of equation A-5. If the usual assumption that H_E is greater than H_A is made, then:

$$H_0 \approx \frac{[(\omega/\gamma)^2 - 2H_E H_A]^{\frac{1}{2}}}{1 - 4\pi\chi} \qquad \text{(A-7)}$$

Case II: $H_0 \| X$, $H_A \| Z$, $N_y = 4\pi$, $N_x = N_z = 0$.
As in Case I, the following polynomial in ω is obtained.

$$\begin{bmatrix} \frac{-i\omega}{\gamma} & 0 & H_A - \lambda M_{20^z} + 4\pi M_{10^z} & (\lambda + 4\pi)M_{10^z} & 0 & 0 \\ 0 & \frac{-i\omega}{\gamma} & (\lambda + 4\pi)M_{20^z} & 4\pi M_{20^z} - \lambda M_{10^z} - H_A & 0 & 0 \\ -H_A + \lambda M_{20^z} & -\lambda M_{10^z} & \frac{-i\omega}{\gamma} & 0 & H_0 - \lambda M_{20^x} & \lambda M_{10^x} \\ -\lambda M_{20^z} & H_A + \lambda M_{10^z} & 0 & \frac{-i\omega}{\gamma} & \lambda M_{20^x} & H_0 - \lambda M_{10^x} \\ 0 & 0 & -4\pi M_{10^x} - H_0 + \lambda M_{20^x} & -(\lambda + 4\pi)M_{10^x} & \frac{-i\omega}{\gamma} & 0 \\ 0 & 0 & -(\lambda + 4\pi)M_{20^x} & -H_0 + \lambda M_{10^x} - 4\pi M_{20^x} & 0 & \frac{-i\omega}{\gamma} \end{bmatrix} = 0 \quad \text{(A-8)}$$

Now make the substitutions $\lambda M_{10^z} = -\lambda M_{20^z} = H_E$, $M_{10^x} = M_{20^x} = (\chi H_0/2)$, and $\lambda \approx (1/\chi_\perp)$. Solution of equation A-8 gives.

$$(\omega/\gamma)^2 = (1 + 4\pi)\, H_0{}^2 + 2(1 + 4\pi\chi)\, H_E H_A + H_A{}^2, \quad \text{(A-9)}$$

$$(\omega/\gamma)^2 = 2H_E H_A + H_A{}^2, \quad \text{(A-10)}$$

$$(\omega/\gamma)^2 = 0. \quad \text{(A-11)}$$

It is noticed that equation A-9 is the only one that contains H_0. Solving it for H_0 gives

$$H_0 = \left[\frac{(\omega/\gamma)^2 - 2(1 + 4\pi\chi)\, H_E H_A - H_A{}^2}{1 + 4\pi\chi}\right]^{\frac{1}{2}} \quad \text{(A-12)}$$

If $4\pi\chi$ in the numerator is dropped because it is small compared with 1, and H_E is assumed to be greater than H_A, then

$$H_0 \approx \left[\frac{(\omega/\gamma)^2 - 2H_E H_A}{1 + 4\pi\chi}\right]^{\frac{1}{2}} \quad \text{(A-13)}$$

Case III:
$H_0 \| H_A \| Z$, $N_x = N_z = 0$, $N_y = 4\pi$. Also $M_{10^y} = M_{20^y} = M_{10^x} = M_{20^x} = 0$.
The polynomial in ω is

$$\begin{bmatrix} \frac{-i\omega}{\gamma} & 0 & H_0 + H_A - \lambda M_{20^z} + 4\pi M_{10^z} & (\lambda + 4\pi)M_{10^z} & 0 & 0 \\ 0 & \frac{-i\omega}{\gamma} & (\lambda + 4\pi)M_{20^z} & H_0 - H_A - \lambda M_{10^z} + 4\pi M_{20^z} & 0 & 0 \\ -H_0 - H_A + \lambda M_{20^z} & -\lambda M_{10^z} & \frac{-i\omega}{\gamma} & 0 & 0 & 0 \\ -\lambda M_{20^z} & -H_0 + H_A + \lambda M_{10^z} & 0 & \frac{-i\omega}{\gamma} & 0 & 0 \\ 0 & 0 & 0 & 0 & -\frac{i\omega}{\gamma} & 0 \\ 0 & 0 & 0 & 0 & 0 & \frac{-i\omega}{\gamma} \end{bmatrix} = 0 \quad \text{(A-14)}$$

Now make the substitutions

$$\lambda(M_{10}{}^z - M_{20}{}^z) = 2H_E \text{ and } M_{10}{}^z + M_{20}{}^z = \chi H_0.$$

This particular case is of interest only when $T < T_N$. Under this condition, χ approaches zero. The solutions of equation A-14 are then

$$(\omega/\gamma)^2 = [H_0 + (2H_E H_A)^{\frac{1}{2}}]^2, \tag{A-15}$$

$$(\omega/\gamma)^2 = [H_0 - (2H_E H_A)^{\frac{1}{2}})^2, \tag{A-16}$$

$$(\omega/\gamma)^2 = 0. \tag{A-17}$$

Solving these equations for positive H_0 gives

$$H_0 = |(\omega/\gamma)^{\frac{1}{2}} \pm (2H_E H_A)^{\frac{1}{2}}| \tag{A-18}$$

The solution observed experimentally was the one with the negative sign.

The intensities of antiferromagnetic resonance lines were shown by Kittel to be comparable to paramagnetic intensities.

APPENDIX B.

Experimental methods. Magnetic Resonance Spectrometer.Because the apparatus used in these experiments is similar to that described by others [19][20], only a brief description is given here. The system is shown schematically in fig. B-1. The sample is placed in a rectangular TE_{011} mode

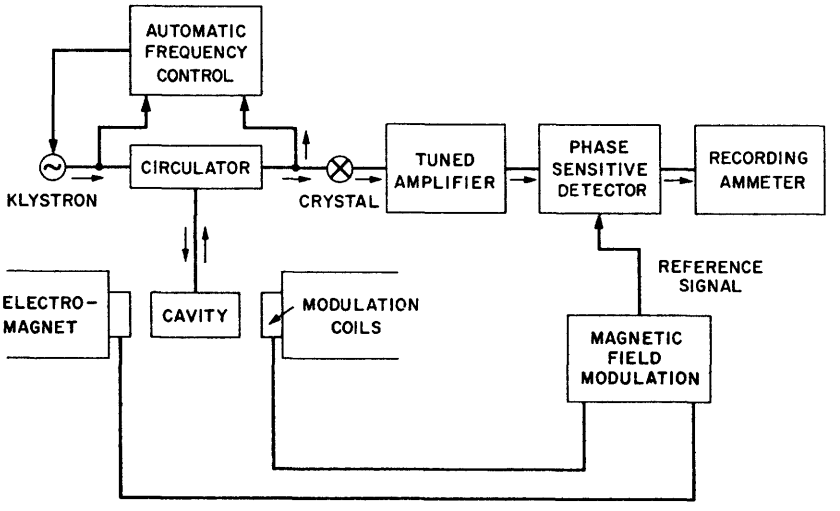

Fig. B-1. Schematic of magnetic resonance spectrometer.

cavity in a region of rf magnetic field that is perpendicular to the external field. The frequency of the klystron is locked by a feedback circuit to the frequency of the cavity to eliminate mixing of the real and imaginary parts of the rf susceptibility.

The resonance is sinusoidally modulated at an audio frequency (50 cycles) and is phase-sensitively detected at the modulation frequency. This type of modulation and detection produces at the output a signal that is proportional to the derivative of the imaginary part of the *rf* susceptibility. The signal is plotted on a recording ammeter as the static field is slowly swept.

Crystal Growing. The method of growing anhydrous single crystals of manganous chloride was similar to that described by Murray [2]). Chemically pure hydrated manganous chloride ($MnCl_2.4H_2O$) was heated in a flowing atmosphere of dry hydrogen chloride gas until the water was driven off. The temperature was then raised above the melting point of the anhydrous compound. The crucible containing the molten compound was then very slowly withdrawn from the heating zone (30 hours). Very good single crystals, of the order of 1 cm^3 in size, were obtained. These crystals, being very hydroscopic, were kept in a desiccator. The crystals were cleaved into thin platelets from which disks were cut. The crystal structure was checked with a Laue *X*-ray photograph of the single crystal and also by means of an *X*-ray analysis of a polycrystalline sample.

Low-Temperature Techniques. A conventional double-dewar system was used, with liquid nitrogen in the outer dewar and liquid helium in the inner dewar. Temperatures in the helium range were measured both by a carbon resistance thermometer [21]) and a vapor pressure thermometer. Above 4.2°K, the resistance thermometer was used exclusively. Temperatures below 4.2°K were controlled in the usual way by regulating the vapor pressure of the liquid helium by means of a vacuum pump.

For temperatures above 4.2°K, a method described by Rose-Innes [22]) was used. It consists of filling the excess space in the bottom of the inner dewar with activated charcoal. Liquid helium is transferred directly into the inner dewar and a normal run is performed. After the liquid helium is gone, the charcoal will have absorbed large quantities of helium gas. The heat of absorption is very high (200–400 cal/gm of helium). This effectively increases the heat capacity of the system, with the result that it will warm up very slowly. The warming-up process can be slowed down, stopped, or reversed by controlling the pumping speed. Data points for temperatures up to 40°K were obtained in this way. It was found that with 15 grams of charcoal, the temperature could be held for as long as 30 minutes at a particular operating point with a total heat leak of approximately 30 milliwatts or more.

Data points at $T = 48$°K were obtained by filling the inner dewar with liquid nitrogen and controlling the vapor pressure with a vacuum pump.

Received 10-8-60

REFERENCES

1) Murray, R. B., and Roberts, L., Phys. Rev. **100** (1955) 1067.
2) Murray, R. B., Phys. Rev. **100** (1955) 1071.
3) Wollan, E. O., e.a., Semiannual Progress Report, ORNL-2430, Physics Division, Oak Ridge National Laboratory, April 8, 1958, p. 65; and Semiannual Progress Report ORNL-2501, June 10, 1958, p. 37.
4) Pauling, L., and Hoard, J. L., Z. Krist **74** (1930) 546.
5) Kittel, C., and Keffer, F., Phys. Rev. **85** (1952) 329.
6) Nagamiya, T., Progr. Theoret. Phys. (Kyoto) **6** (1951) 342.
7) Van Vleck, J. H., Phys. Rev. **74** (1948) 1168.
8) Ishiguro, E., Kambe, K., Usui, T., Physica **17** (1951) 310.
9) Anderson, P. W., and Weiss, P. R., Rev. Mod. Phys. **25** (1953) 269.
10) Kubo, R., and Tomita, K., J. Phys. Soc. Japan **9** (1954) 888.
11) Yokota, M., J. Phys. Soc. Japan **10** (1955) 762.
12) Abe, H., Ono, K., and Shimoda, J., Phys. Rev. **92** (1953) 551.
13) Rogers, R. N., Anderson, M. E., and Pake, G. E., Bull. Am. Phys. Soc. II (1959) 261.
14) Pryce, M. H. L., and Stevens, K. W. H., Proc. Phys. Soc. (London) **A 63** (1950) 39.
15) Nethercot, A. H., and Johnson, F. M. Phys. Rev. **114** (1959) 705.
16) Gerritsen, H., Garber, M., and Drews, G., Physica **22** (1956) 213.
17) Orbach, R., and Pincus, P., Phys. Rev. **113** (1959) 1213.
18) Kittel, C., Introduction to Solid State Physics (John Wiley and Sons, Inc., New York, 1956).
19) Wolga, G., Ph. D., Thesis, Department of Physics, M.I.T., 1957, Appendix i.
20) Strandberg, M. W. P., Tinkham, M., Solt, I. H., Jr., and Davis, C. F., Jr., Rev. Sci. Instr. **27** (1956) 596.
21) Clement, J. R. and Quinnell, E. H., Rev. Sci. Instr. **23** (1952) 213.
22) Rose-Innes, A. C., and Bromm, R. F., J. Sci. Instr. **33** (1956) 31.